Highly Sensitive Nano-Biosensor Based on a Binary Photonic Crystal for Cancer Cell Detection

Malek G. Daher
Islamic University of Gaza
Sofyan A. Taya (staya@iugaza.edu.ps)
Islamic University of Gaza https://orcid.org/0000-0001-5060-2534
Ilhami Colak
Nisantasi University: Nisantasi Universitesi
Shobhit K. Patel
Marwadi University
Omar M. Ramahi
University of Waterloo

Research Article

Keywords: Binary photonic crystal, cancer cell, sensor, defect mode, quality factor

Posted Date: March 11th, 2022

DOI: https://doi.org/10.21203/rs.3.rs-1218966/v1

Highly sensitive nano-biosensor based on a binary photonic crystal for cancer cell detection

Malek G. Daher[1], Sofyan A. Taya[1,2*], Ilhami Colak[3], Shobhit K. Patel[4], Omar M. Ramahi[2]

[1]Physics Department, Islamic University of Gaza, P.O. Box 108, Gaza, Palestine.
[2]Department of Electrical and Computer Engineering, University of Waterloo, 200 University Avenue West, Waterloo, Ontario N2L 3G1, Canada.
[3]Department of Electrical and Electronics Engineering, Nisantasi University, Istanbul, Turkey
[4]Department of Computer Engineering, Marwadi University, Rajkot-360003, India.

*Corresponding Author:
Sofyan A. Taya
email: staya@iugaza.edu.ps
email: staya@uwaterloo.ca

Abstract

Today, cancer disease is a significant reason for the death of many patients. In many cases, cancer is diagnosed after metastasized during the body. Thus, the earlier detection gives a better opportunity for treatment and cure. A simple 1-D binary photonic crystal with a defect layer is proposed with the structure $(Si/\ SiO_2)^N$/Defect/$(Si/\ SiO_2)^N$ as a detector for cancerous cells. The defect layer is taken here as the patient's blood sample. Compared with the normal blood sample, the cancerous samples lead to a considerable change in the refractive index. This index variation leads to a shift in the resonant mode position which can be used to diagnose cancer cells. The transfer matrix method is employed to analyze the structure. The number of periods, defect layer thickness and incident angle are investigated to maximize the sensitivity. The sensitivity is calculated at optimized conditions and found as 2400.08 nm/RIU. This sensitivity is extremely high when compared to the most recent biosensors. All the sensor performance parameters are calculated and discussed.

Keywords: Binary photonic crystal, cancer cell, sensor, defect mode, quality factor.

1. Introduction:

Due to medical science's failure to provide a complete treatment for cancer disorders, cancer diagnosis research has gotten a lot of attention during the previous several decades all over the world. These malignant cells grow abnormally and form tumours, which can be detected by a variety of medical tests. To reduce the deadly effects of cancer, it is critical to discover it at an early stage and to do so, a variety of clinical investigations are available in healthcare organisations to anticipate the current cell report [1]. However, understanding the optical, chemical, and mechanical properties of a living cancer cell can lead to numerous interesting new insights into the cell's biology [2]. The interaction of light with cells has recently yielded useful knowledge about changes in optical characteristics of various cells. Most crucially, the cell's refractive index has gotten a lot of attention, which has expanded the possibilities for detecting cell abnormalities. According to cancer science, normal cells' refractive indices are lower than cancerous cells', which can be used as a useful indicator in the identification and diagnosis of malignant cells [3].

Photonic sensors are specifically intended to detect a variety of bio analytes by successfully converting the bio-entity into an electrical form that can be examined using a spectrometer [4]. Electrical characteristics and electric field analysis are used to examine the differences between normal and malignant cells [5]. Furthermore, the refractive indices of various analytes emerge as a critical parameter in the development of precise biosensors [6-8]. Recently, a few studies have been published that are based on the tabular optical properties of a variety of tissues, but this table may not provide enough information about living cells. The effective refractive index of discrete live cells has been determined using several optical [9,10] approaches such as solution matching [11] and refractometry analysis [12]. Even though the aforementioned references reveal fascinating results, the paucity of research on the cell's local refractive index is a matter of concern. Furthermore, the sensing devices and procedures are somewhat sophisticated in terms of design, making them challenging to implement in practice. Apart from that, none of the studies in the literature has looked at sensor sensitivity, resolution, quality factor, and nonlinear coefficient all at the same time. Furthermore, the aforementioned sensor measurement parameters are insufficient to satisfy the current sensing scenario's difficulty. Although there are various strategies for detecting cancer cells in the literature, the current study is based on an examination of a binary photonic crystal for detecting normal and cancerous cells in a short amount of time. In a recent work, the authors have analysed the sensing of cancerous cells by investigating electric field distribution in a simple 2D photonic crystal fiber structure. Two clusters of cell lines, human immortalized normal oral keratinocyte which in normal cells group and YD-10B cells which are cancerous, were considered [13].

In this work, simple methodologies and compact structures are employed which can be easily implemented with newly emerging technologies. Normal cells, as well as five caner cells, are considered. Jurkat, Hela, PC12, MDA-MB231 and MCF-7 cancer cells are treated as analytes. The sensor performance parameters are all considered such as quality factor, figure of merit, detection limit, detection accuracy, signal-to-noise ratio, standard deviation, sensor resolution and dynamic range to enhance the novelty of the current research.

2. Design and theoretical model

One-dimensional (1D) binary defective photonic crystal is proposed for cancer cell detection. The photonic crystal has the structure $(AB)^N/D/(AB)^N$. Layers A and B are chosen as Si and SiO_2, respectively. D is the defect layer which is either a normal or cancerous cell. Layer D lies midway between two identical period numbers (N). The thicknesses and refractive indices of the layers are d_1, d_2 and d_D and n_1, n_2, and n_D, for Si, SiO_2 and the defect layers, respectively.

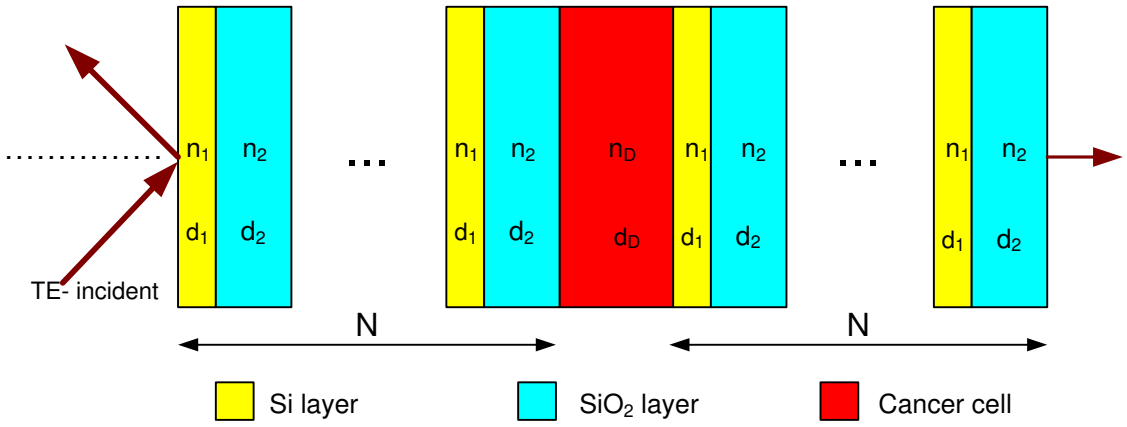

Fig. 1. Schematic diagram of 1D binary photonic crystal having a cancer cell as a defect layer.

A wide choice of different techniques to simulate photonic crystals is described in the literature. In the specific case of 1D photonic crystals, the transmission spectrum can be simulated using many different numerical methods such as finite difference time domain methods and finite element methods. The transfer matrix method is a simple and flexible technique to analyze the optical properties of 1D photonic crystals. We consider a system consisting of air/multilayer/substrate. The parameters related to air and substrate media are just their refractive indexes, n_o and n_s, respectively. With E_s and H_s are the electric and magnetic fields in the substrate, we can write the incident fields (E_0 and H_0) in terms of E_s and H_s as

$$\begin{bmatrix} \mathrm{E}_0 \\ \mathrm{H}_0 \end{bmatrix} = \prod_{j=1}^{N} F_j \begin{bmatrix} \mathrm{Es} \\ \mathrm{Hs} \end{bmatrix} = \begin{bmatrix} f_{11} & f_{12} \\ f_{21} & f_{22} \end{bmatrix} \begin{bmatrix} \mathrm{Es} \\ \mathrm{Hs} \end{bmatrix} \tag{1}$$

where F_j is the characteristic matrix of one layer and f_{ij} are the matrix elements. F_j can be written as

$$F_j = \begin{bmatrix} \cos(\delta_j) & -\frac{i \sin(\delta_j)}{\gamma_j} \\ -i\,\gamma_j \sin(\delta_j) & \cos(\delta_j) \end{bmatrix} \tag{2}$$

δ_j is the phase variation of the light wave due to propagating through the j^{th} layer

$$\delta_j = \frac{2\pi}{\lambda} n_j d_j \cos\theta_j \tag{3}$$

where n_j, d_j θ_j are the refractive index, thickness and angle of incidence of the layer. θ_j can be written in terms of the initial incidence angle θ_0 as

$$\cos\theta_j = \sqrt{1 - \left(\frac{n_0 \sin(\theta_0)}{n_j}\right)^2} \tag{4}$$

$\gamma_j = n_j \cos(\theta_j)$ in transverse electric (TE) wave whereas $\gamma_j = \cos(\theta_j)/n_j$ in transverse magnetic (TM) wave and n_0 is the refractive index of the incidence medium. The transfer matrix F_0 for one period consisting of two layers A and B can be written as $F_0 = F_A F_B$. The full transfer matrix F of a defective binary photonic crystal can be expressed as

$$F = (F_0)^N F_D (F_0)^N = \begin{bmatrix} F_{11} & F_{12} \\ F_{21} & F_{22} \end{bmatrix} \tag{5}$$

where F_D is the transfer matrix of the defect layer and F_{ij} are the elements of the total transfer matrix F.
The transmission coefficient can be written as

$$t = \frac{2\gamma_{in}}{(F_{11}+F_{12}\,\gamma_{out})\gamma_{in}+(F_{21}+F_{22}\,\gamma_{out})} \quad (6)$$

and the transmittance can have the form

$$T = \frac{\gamma_{out}}{\gamma_{in}}|t|^2 \quad (7)$$

The reflection coefficient can be written as

$$r = \frac{(F_{11}+F_{12}\gamma_{out})\gamma_{in}-(F_{21}+F_{22}\gamma_{out})}{(F_{11}+F_{12}\gamma_{out})\gamma_{in}+(F_{21}+F_{22}\gamma_{out})} \quad (8)$$

and the reflectance can have the form

$$R = |r|^2 \quad (9)$$

For transverse electric (TE) waves, $\gamma_{in} = \gamma_{out} = \cos(\theta_0)$ since the binary photonic crystal is assumed to be surrounded by air.
Based on above theoretical equations, properties of both photonic bandgap and defect mode of a defective binary photonic crystal can be investigated.

3. Results and Discussion

3.1 Cancer cell sensor

A binary photonic crystal is assumed with the structure $(Si/SiO_2)^N/D/(Si/SiO_2)^N$ whose refractive indices are 3.3 for the Si and 1.46 for the SiO_2. The thicknesses of the layers are taken as $d_1 = 117\ nm$ and $d_2 = 265$ nm, respectively. The wavelength of the incident radiation is taken from 800 nm to 2300 nm and the number of periods is taken as $N = 5$. Normal incidence is first considered in which $\theta_0 = 0$ and D is either the normal or cancerous cell. The transmission spectrum through the proposed binary photonic crystal without any defect layer is shown in Fig. 2a. A photonic bandgap of width 890 nm can be seen with left and right edges are at wavelengths of 1221 nm and 2111, respectively. Figure 2b shows the transmission spectrum through the structure when the normal cell layer of thickness 1D is treated as a defect layer, where $D = d_1 + d_2$ ($d_1 = 117$ nm, $d_2 = 265$ nm). The width of the photonic bandgap becomes 1016.01 nm where the left and right edges are at wavelengths of 1202 nm and 2218.01 nm, respectively. A defect mode can be seen in the figure at a resonant wavelength of 1685.54 nm. An enlarged view of the defect mode is plotted in Fig. 2c when the normal cell layer is treated as a defect layer. The full width at half maximum of the resonant peak is $FWHM = 0.45\ nm$ where the wavelength of left and right edges at half maximum are at 1685.31 nm and 1685.76 nm. The quality factor (QF) is found as 3745.64 which was calculated by the following equation: $QF = \frac{\lambda_{peak}}{FWHM}$, where λ_{peak} is the resonant wavelength.

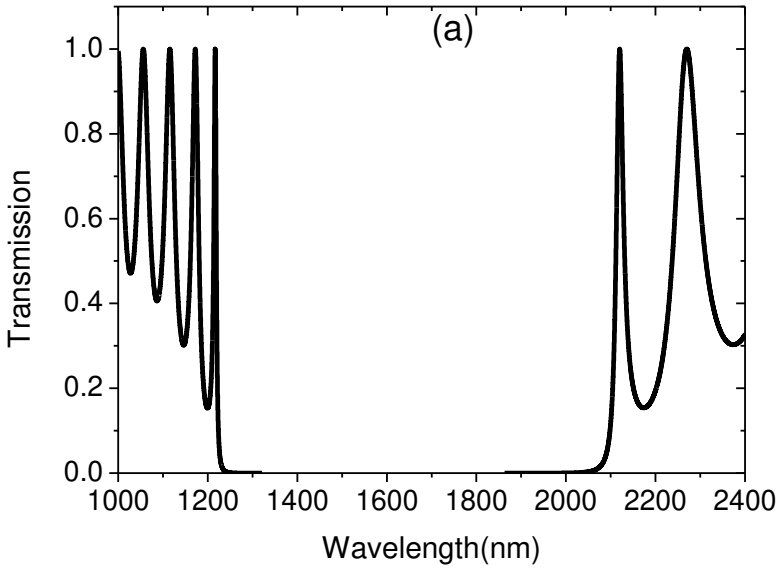
(a)
Transmission
1.0
0.8
0.6
0.4
0.2
0.0
1000
1200
1400
1600
1800
2000
2200
2400
Wavelength(nm)

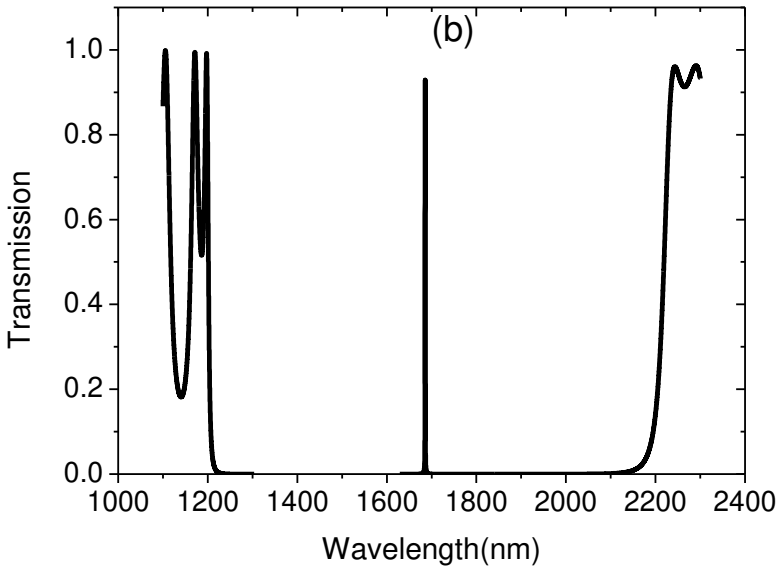
(b)
Transmission
1.0
0.8
0.6
0.4
0.2
0.0
1000
1200
1400
1600
1800
2000
2200
2400
Wavelength(nm)

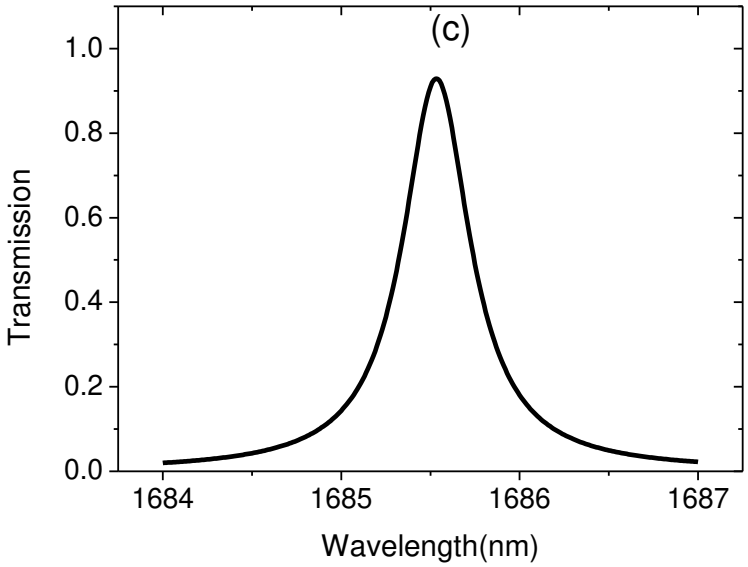

Fig. 2. Transmission spectra of a binary photonic crystal without a defect layer (a), with a defect layer (b) and an enlarged view of the defect mode (c) for TE wave at $\theta_0 = 0.0°$, $d_1 = 117$ nm, $d_2 = 265$ nm, $n_1 = 3.3$, $n_2 = 1.46$ and $N = 5$.

Figure 3 shows the transmission spectra through the binary photonic crystal when the cancerous cells are treated as defect layers. It was found that resonant peak shifts to higher wavelength region. The new wavelength positions of the defect mode are cell-dependent. The new wavelength positions are at 1702.92, 1703.8, 1705.10, 1706.85 and 1707.71 nm for Jurkat, Hela, PC12, MDA-MB231 and MCF-7 cells, respectively. The sensitivity can be calculated as $\frac{\Delta\lambda}{\Delta n}$, where $\Delta\lambda$ is the wavelength shift between the resonant peak position of the normal cell and cancer cell and Δn is the change of refractive index between the normal cell and cancer cell. The sensitivity was found as 434.5, 434.76, 434.66, 434.89 and 434.70 nm/RIU for the cells of Jurkat, Hela, PC12, MDA-MB231 and MCF-7, respectively. Table 1 presents the refractive indices of different cancerous cells, defect mode positions of each and the sensitivity of the proposed binary photonic crystal to each cell.

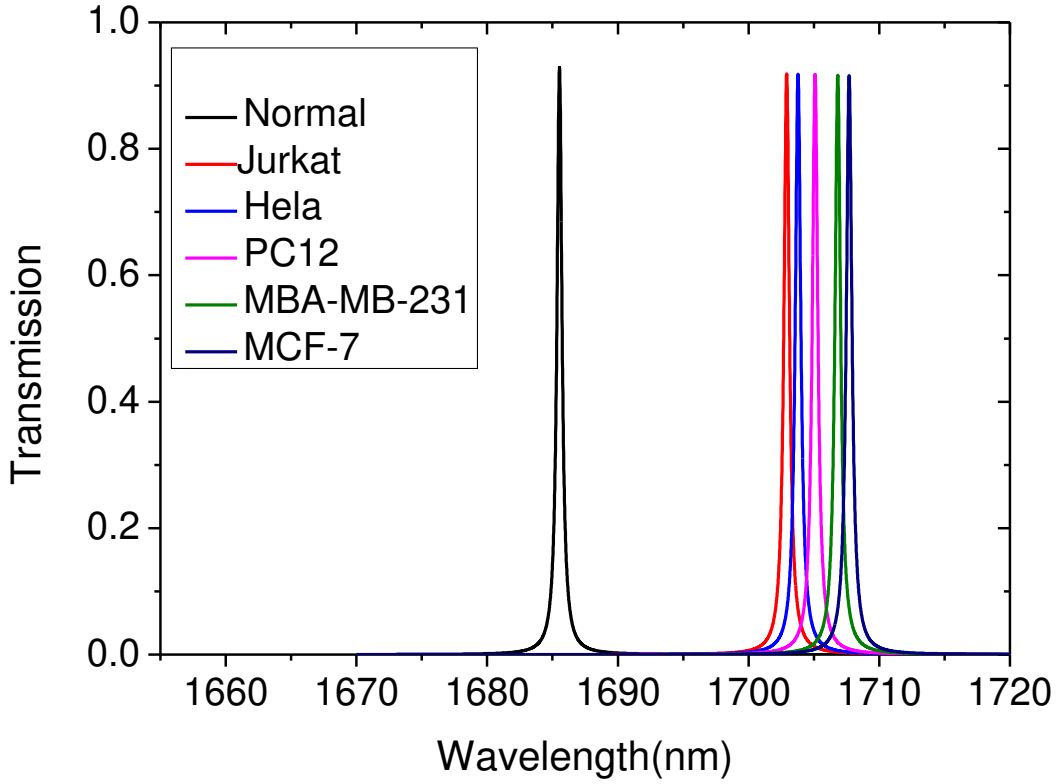

Fig. 3. Transmission spectra of a binary photonic crystal for TE wave at $\theta_0 = 0.0°$, $d_1 = 117$ nm, $d_2 = 265$ nm, $n_1 = 3.3$, $n_2 = 1.46$, d = 1D and N = 5.

Table 1. Defect mode position and sensitivity of the cancerous cells at $\theta_0 = 0.0°$, $d_1 = 117$ nm, $d_2 = 265$ nm, $n_1 = 3.3$, $n_2 = 1.46$, d = 1D and N = 5.

Cell	Refractive index	Wavelength (nm)	Wavelength shift (nm)	Sensitivity (nm/RIU)
Normal	1.350	1685.54	-	-
Jurkat	1.390	1702.92	17.38	434.5
Hela	1.392	1703.8	18.26	434.76
PC12	1.395	1705.10	19.56	434.66
MDA-MB231	1.399	1706.85	21.31	434.89
MCF-7	1.401	1707.71	22.17	434.70

3.2 Effect of the incident angle

3.2.1 Angle of incidence and sensitivity

The incident angle variation has an essential effect on the bandgap position according to the Bragg-Snell law [14]

$$m\lambda = 2\,d\sqrt{n_{eff}^2 - \sin^2\theta_0} \qquad (10)$$

where m, λ, d, θ_0 and n_{eff} are the order of diffraction (m is an integer), the free space wavelength, the interplanar spacing, the incident angle, the effective refractive index, respectively. The angle of incidence was changed from 0 to 89° in steps of 5°. The results of two angles are presented in Tables 2 and 3 which show the enhancement of sensitivity from 496.77 nm/RIU to 671.23 nm/RIU when the incident angle increases from 30° to 60°.

Table 2. Defect mode position and sensitivity of the cancerous cells at an incidence angle of θ_0 = 30°.

Cell	Refractive index	Wavelength (nm)	Wavelength shift (nm)	Sensitivity (nm/RIU)
Normal	1.350	1604.59	-	-
Jurkat	1.390	1624.46	19.87	496.75
Hela	1.392	1625.46	20.87	496.90
PC12	1.395	1626.93	22.34	496.44
MDA-MB231	1.399	1628.94	24.35	496.93
MCF-7	1.401	1629.93	25.34	496.84
Average sensitivity = 496.77 nm/RIU				

Table 3. Defect mode position and sensitivity of the cancerous cells at an incidence angle of θ_0 = 60°.

Cell	Refractive index	Wavelength (nm)	Wavelength shift (nm)	Sensitivity (nm/RIU)
Normal	1.350	1411	-	-
Jurkat	1.390	1437.85	26.85	671.25
Hela	1.392	1439.2	28.2	671.42
PC12	1.395	1441.2	30.2	671.11
MDA-MB231	1.399	1443.89	32.89	671.22
MCF-7	1.401	1445.23	34.23	671.17
Average sensitivity = 671.23 nm/RIU				

In Table 4, we calculated the average sensitivity of the proposed binary photonic crystal corresponding to different incident angles starting from θ_0 = 0° to θ_0 = 89° with an increment of 5°. The sensitivity attains a considerable enhancement as the incident angle increases from 0° to 85°. For further increase of the angle of incidence beyond 85°, insignificant enhancement of the sensitivity can be observed. So, the angle of 85° is taken as the optimum value of the incident angle. The relation between the sensitivity (S) to cancer cells and the incident angle (θ_0) of a proposed binary photonic crystal is shown in Fig. 4 (blue points). It can be fitted by the following equation

$$S(\theta_0) = 434.08 + 0.3482\theta_0 + 0.03322\theta_0^2 + 1.17\theta_0^3 - 1.2131 \times 10^{-5}\theta_0^4 \qquad (11)$$

The fitting equation (11) is useful to predict the sensitivity of cancer cell sensor at any value of the incident angle located between $\theta_0 = 0.0°$ and $\theta_0 = 85°$. The fitted sensitivity as a function of the

incident angle (red curve) along with the data (blue points) is shown in Fig.4. The matching between the data and the fitting equation is perfect.

Table 4. Effect of the incident angle on the sensitivity of the cancerous cells at d = 1D and N = 5.

Incident angle (degree)	Average sensitivity (nm/RIU)
0	434.7
5	436.21
10	441.23
15	450.08
20	462.11
25	477.49
30	496.77
35	519.47
40	545.2
45	573.73
50	604.75
55	637.26
60	671.23
65	702.81
70	733.39
75	758.39
80	778.23
85	790.45
89	794.69

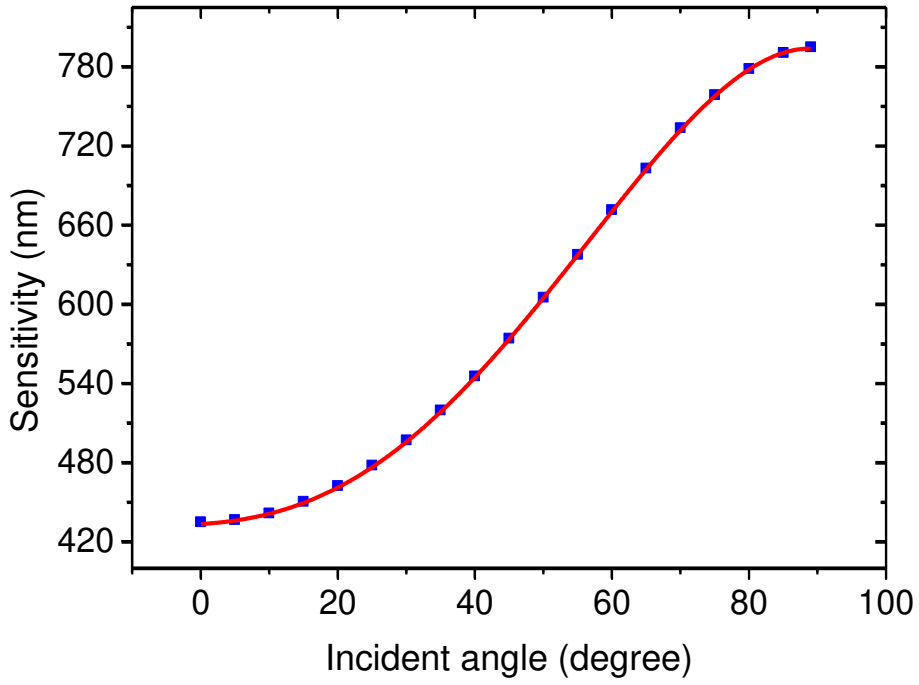

Fig. 4. Sensitivity with the angle of incidence of a binary photonic crystal for TE wave at d_1 = 117 nm, d_2 = 265 nm, n_1 = 3.3, n_2 = 1.46, d = 1D and N = 5.

3.2.2 Angle of incidence and photonic bandgap

The photonic bandgap can be explained by the transmission of light through certain frequencies is zero by multiple Bragg scattering. The results in Table 5 show that as the incident angle increases, the photonic bandgap width increases. At an incident angle of 0.0°, the photonic bandgap width is 1016.01 nm. When the incident angle increases to 89°, the photonic bandgap width increases to be 1094.7 nm. The photonic bandgap width versus the incident angle is shown in Fig. 5. The photonic bandgap width is calculated as the difference between the wavelengths of the left and right edges at half maximum of transmission in nanometers.

Table 5. Effect of the incident angle on the width of bandgap at d = 1D and N = 5.

Incident angle (degree)	Left band edge (nm)	Right band edge (nm)	Half band width (nm)
0	1202	2218.01	1016.01
5	1200.1	2217.8	1017.7
10	1195.18	2214.15	1018.97
15	1187	2208.55	1021.55
20	1175.52	2200	1024.48
25	1161.59	2189.89	1028.3
30	1144.79	2178	1033.21

35	1127	2164.6	1037.6
40	1107.4	2150.8	1043.4
45	1086.4	2136	1049.6
50	1065.02	2121.3	1056.28
55	1044.66	2107.8	1063.14
60	1025.24	2095	1069.76
65	1007	2082	1075
70	992	2072.24	1080.24
75	978	2064	1086
80	969.9	2058.6	1088.7
85	964	2056.7	1092.7
89	962	2056.7	1094.7

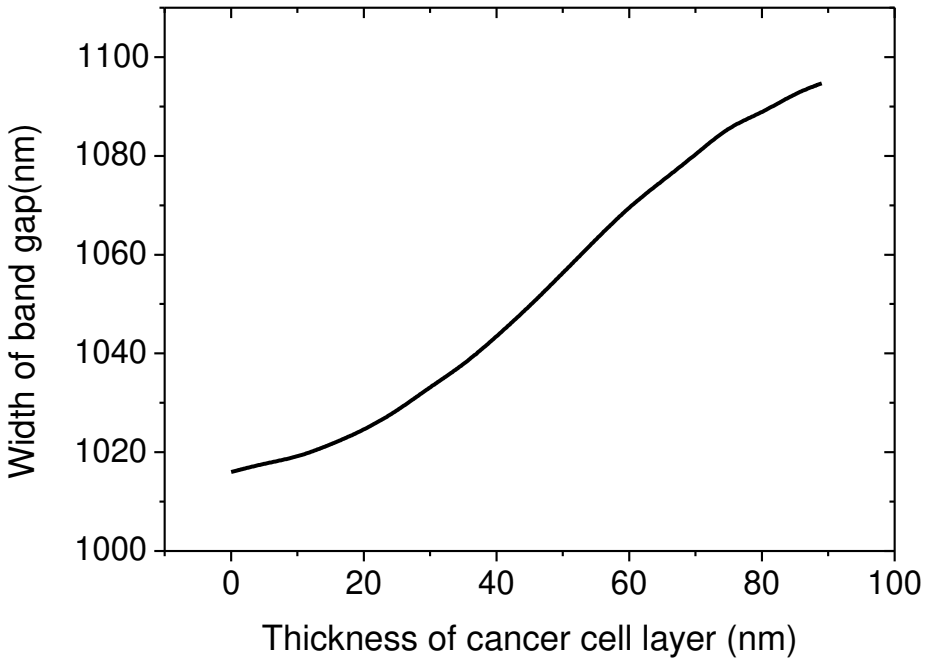

Fig. 5. Width of bandgap versus the incident angle of a binary photonic crystal for TE wave at d_1 = 117 nm, d_2 = 265 nm, n_1 = 3.3, n_2 = 1.46, d = 1D and N = 5.

3.3 Effect of the number of periods

The number of periods of a photonic crystal can affect the sensitivity and bandgap width of a binary photonic crystal.

3.3.1 Number of periods and sensitivity

The number of periods was changed from 3 to 7. Some of the results can be seen in Tables 6 and 7. The average sensitivity has dropped from 444.45 nm/RIU to 434.27 nm/RIU as the number of

periods increases from 3 to 6. The resonant peak position is 1687.65 nm when the normal cell is treated as a defect layer at a number of periods of 3. But when the cancerous cells are treated as defect layers, it is found that resonant peak shifts to a higher wavelength region (redshift) as shown in Fig.6. The new wavelength positions are at 1705.44, 1706.31, 1707.66, 1709.41and 1710.32 nm for Jurkat, Hela, PC12, MDA-MB231 and MCF-7 cells, respectively. The sensitivity is calculated and found as 444.75, 444.28, 444.66, 444.08 and 444.50 nm/RIU for the cells of Jurkat, Hela, PC12, MDA-MB231 and MCF-7, respectively.

Table 6. Defect mode position and sensitivity of the cancerous cells at a number of period N = 3.

Cell	Refractive index	Wavelength (nm)	Wavelength shift (nm)	Sensitivity (nm/RIU)
Normal	1.350	1687.65	-	-
Jurkat	1.390	1705.44	17.79	444.75
Hela	1.392	1706.31	18.66	444.28
PC12	1.395	1707.66	20.01	444.66
MDA-MB231	1.399	1709.41	21.76	444.08
MCF-7	1.401	1710.32	22.67	444.50
Average sensitivity = 444.45 nm/RIU				

Table 7. Defect mode position and sensitivity of the cancerous cells at a number of period N = 6.

Cell	Refractive index	Wavelength (nm)	Wavelength shift (nm)	Sensitivity (nm/RIU)
Normal	1.350	1685.46	-	-
Jurkat	1.390	1702.83	17.37	434.25
Hela	1.392	1703.71	18.25	434.52
PC12	1.395	1705	19.54	434.22
MDA-MB231	1.399	1706.74	21.28	434.28
MCF-7	1.401	1707.6	22.14	434.11
Average sensitivity = 434.27 nm/RIU				

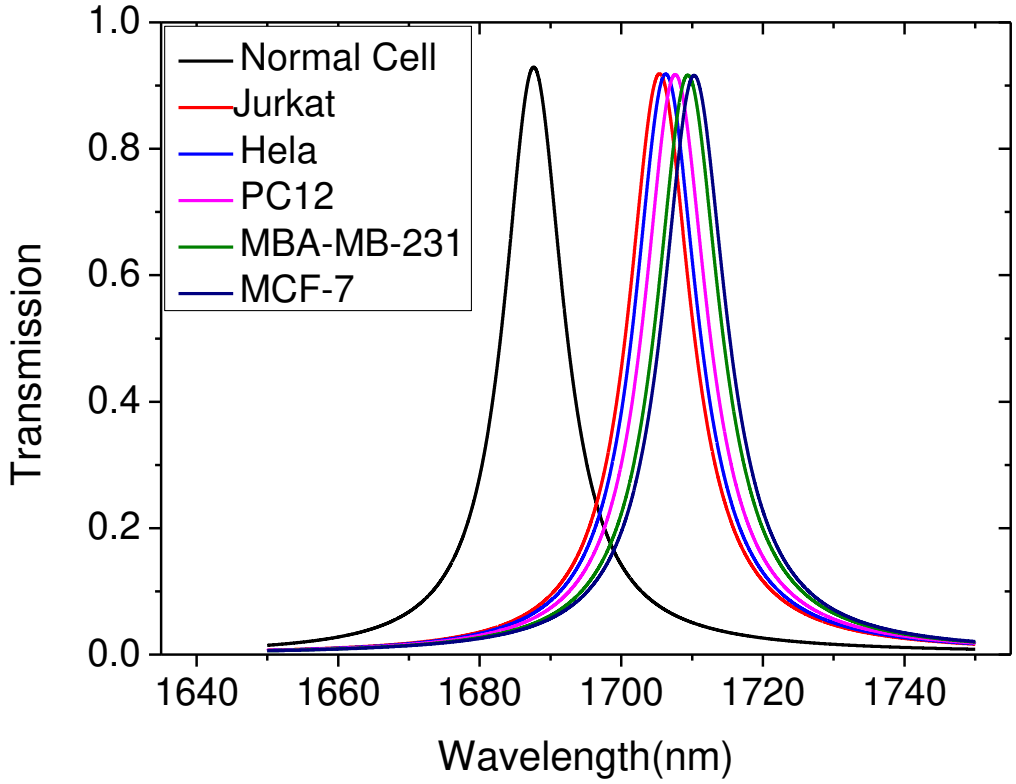

Fig. 6. Transmission spectra of a binary photonic crystal for TE wave at $\theta_0 = 0.0°$, $d_1 = 117$ nm, $d_2 = 265$ nm, $n_1 = 3.3$, $n_2 = 1.46$, d = 1D and N = 3.

Table 8 shows that as the number of periods increases, the sensitivity of the biosensor decreases. This can be attributed to the fraction of light in the analyte layer is less when the number of periods increases. The relation between the sensitivity of cancer cell sensor (S) and the number of periods (N) of a proposed binary photonic crystal can be fitted by the following equation

$$S(N) = 644.05 - 149.028N + 39.6608N^2 - 4.66667N^3 + 0.204167N^4 \qquad (12)$$

The fitting equation (12) can predict the sensitivity of the cancer cell sensor at any value of the number of periods located between $N = 3$ and N = 7. When the number of periods increases beyond N = 7, the defect mode starts vanishing. The fitting equation of the sensitivity as a function of the number of periods (red curve) along with the data (blue points) is shown in Fig.7. The matching between the data and the fitting equations is perfect.

Table 8. Effect of the number of periods on the sensitivity of the cancerous cells at d = 1D and $\theta_0 = 0°$.

Number of Periods (N)	Average sensitivity (nm/RIU)

3	444.45
4	436.11
5	434.70
6	434.27
7	433.77

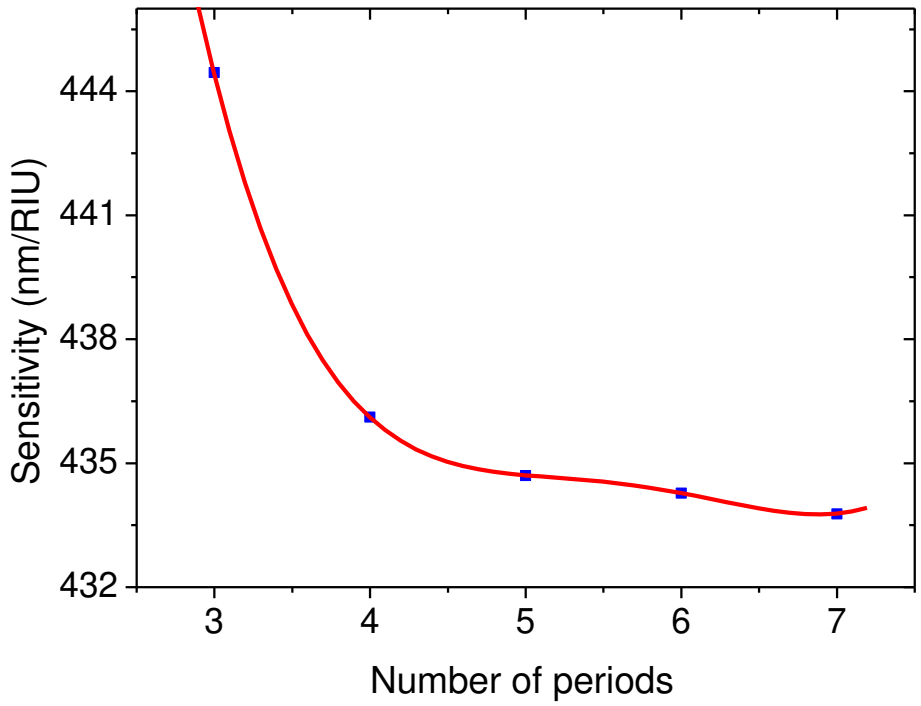

Fig. 7. Sensitivity versus the number of periods of a binary photonic crystal for TE wave at d_1 = 117 nm, d_2 = 265 nm, n_1 = 3.3, n_2 = 1.46, θ_0 = 0.0° and d = 1D.

3.3.2 Number of periods and photonic bandgap

Table 9 presents the bandgap width of the proposed binary photonic crystal and the wavelength positions of the left and right edges at different N starting from N = 3 to N = 10. When the number of periods increases the photonic bandgap width decreases. For a binary photonic crystal and at N = 3, the photonic bandgap width is 1246 nm. When N becomes 10, the photonic bandgap width decreases to be 889.4 nm. When N is less than 3, the photonic bandgap cannot be observed. The bandgap width versus the number of periods is shown in Fig. 8.

Table 9. Effect of the number of periods on the bandgap width at d = 1D and θ_0 = 0°.

Number of periods	Left band edge (nm)	Right band edge (nm)	Half band width (nm)
3	1172	2418	1246
4	1191.3	2287.7	1096.4
5	1202	2220	1018

6	1209	2178.5	969.5
7	1214.62	2152.4	937.78
8	1219	2134.7	915.7
9	1220	2122	902
10	1222	2111.4	889.4

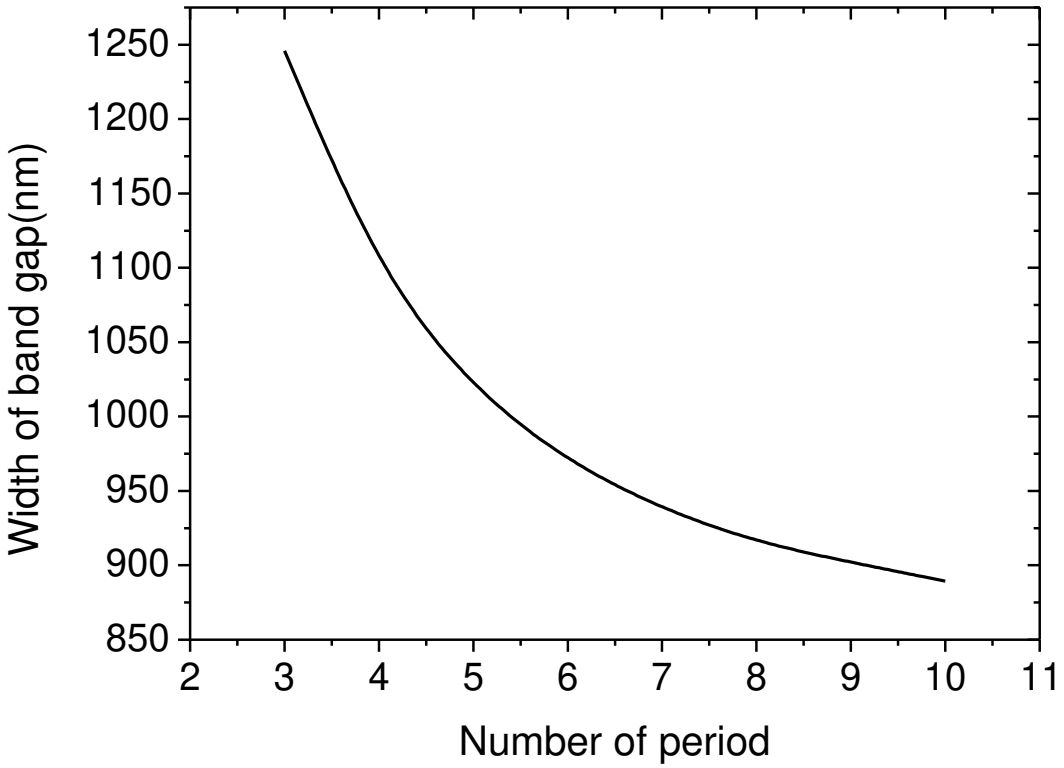

Fig. 8. Width of bandgap versus the number of periods of a binary photonic crystal for TE wave at d_1 = 117 nm, d_2 = 265 nm, n_1 = 3.3, n_2 = 1.46, θ_0 = 0.0° and d = 1D

3.4. Effect of cancer cell layer thickness

3.4.1. Cancer cell layer thickness and sensitivity

The cancer cell layer thickness was changed from 1D to 13D. Some of the results can be seen in Tables 10 and 11. The average sensitivity has risen from 434.7 nm/RIU to 802.55 nm/RIU as the cancer cell layer thickness increases from 1D to 4D. Table 12 shows that as the cancer cell layer thickness increases the sensitivity of the biosensor is dramatically enhanced. In optimizing the proposed sensor, we consider the cancer cell layer thickness to be 13D. The relation between the

sensitivity and the cancer cell layer thickness of a proposed binary photonic crystal can be fitted by the following equation

$$S(d_f) = 201.7 + 0.62d_f - 1.7046 \times 10^{-4} d_f^2 + 2.2 \times 10^{-8} d_f^3 - 1.01 \times 10^{-12} d_f^4 \qquad (13)$$

The fitted sensitivity as a function of cancer cell layer thickness (red curve) along with the data presented in Table 12 (blue points) is shown in Fig. 9. The matching between the calculated data and the fitting equations is excellent.

Table 10. Defect mode positions and sensitivity at a cancer cell layer thickness of 1D.

Cell	Refractive index	Wavelength (nm)	Wavelength shift (nm)	Sensitivity (nm/RIU)
Normal	1.350	1685.54	-	-
Jurkat	1.390	1702.92	17.38	434.5
Hela	1.392	1703.8	18.26	434.76
PC12	1.395	1705.10	19.56	434.66
MDA-MB231	1.399	1706.85	21.31	434.89
MCF-7	1.401	1707.71	22.17	434.70
Average sensitivity = 434.7 nm/RIU				

Table 11. Defect mode positions and sensitivity at a cancer cell layer thickness of 4D.

Cell	Refractive index	Wavelength (nm)	Wavelength shift (nm)	Sensitivity (nm/RIU)
Normal	1.350	1613.99	-	-
Jurkat	1.390	1646.09	32.1	802.5
Hela	1.392	1647.71	33.72	802.85
PC12	1.395	1650.1	36.11	802.44
MDA-MB231	1.399	1653.33	39.34	802.85
MCF-7	1.401	1654.9	40.91	802.15
Average sensitivity = 802.55 nm/RIU				

Table 12. Effect of the cancer cell layer thickness on the cancerous cell sensitivity at $\theta_0 = 0°$ and N = 5.

Defect layer thickness (nm)	Average sensitivity (nm/RIU)
1D	434.7
2D	524.60
3D	775.17
4D	802.55
5D	925.58

6D	945.57
7D	1014.87
8D	1032.72
9D	1076.09
10D	1092.36
11D	1120.64
12D	1136.24
13D	1156.75

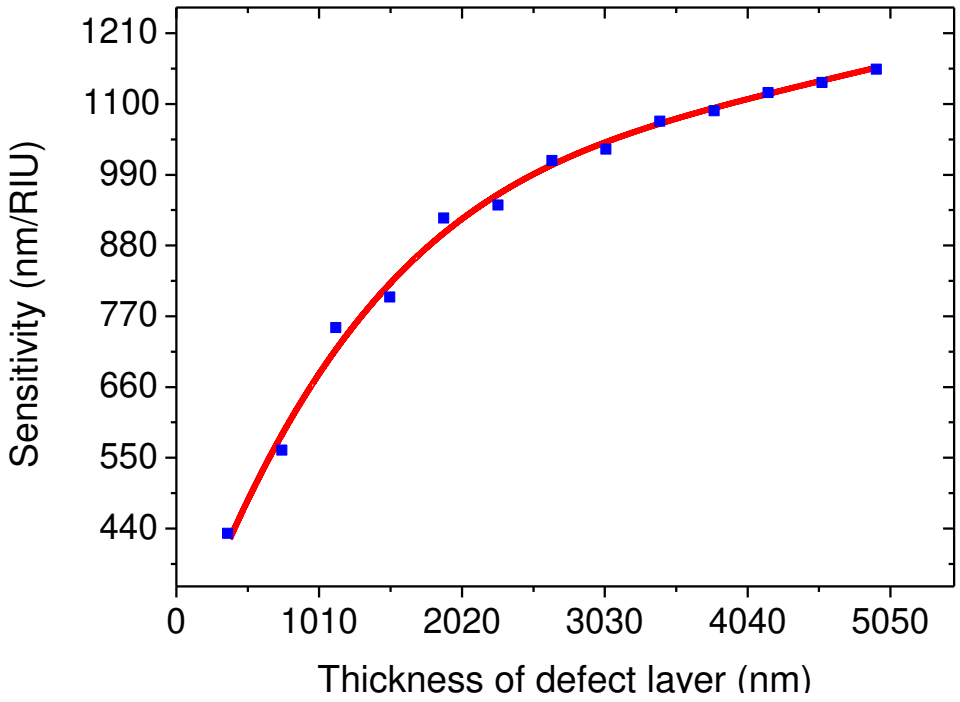

Fig. 9. Sensitivity versus the cancer cell layer thickness of a binary photonic crystal for TE wave at d_1 = 117 nm, d_2 = 265 nm, n_1 = 3.3, n_2 = 1.46, $\theta_0 = 0°$ and N = 5.

3.4.2 Cancer cell layer thickness and photonic bandgap

Table 13 shows that the photonic bandgap width oscillates as the cancer cell layer thickness increases. For example, as the cancer cell layer thickness increases from 1D to 2D, the photonic bandgap width decreases from 1018 nm to 905.2 nm and as the layer thickness increases from 2D to 3D, the photonic bandgap width increases from 905.2 nm to 1024 nm. The photonic bandgap width versus the cancer cell layer thickness is plotted in Fig. 10.

Table 13. Effect of the cancer cell layer thickness on the bandgap width at $\theta_0 = 0°$ and N = 5.

Defect layer thickness (nm)	Initial wavelength (nm)	Final wavelength (nm)	Width of bandgap (nm)
1D	1202	2220	1018
2D	1193.8	2099	905.2
3D	1188	2212	1024
4D	1185.7	2094	908.3
5D	1183.5	2205.2	1021.7
6D	1228	2089	861
7D	1211	2197	986
8D	1203	2085.2	882.2
9D	1194.82	2189.3	994.48
10D	1190.3	2082.85	992.55
11D	1187	2181.28	994.28
12D	1231	2080.6	849.6
13D	1218	2173.46	955.46

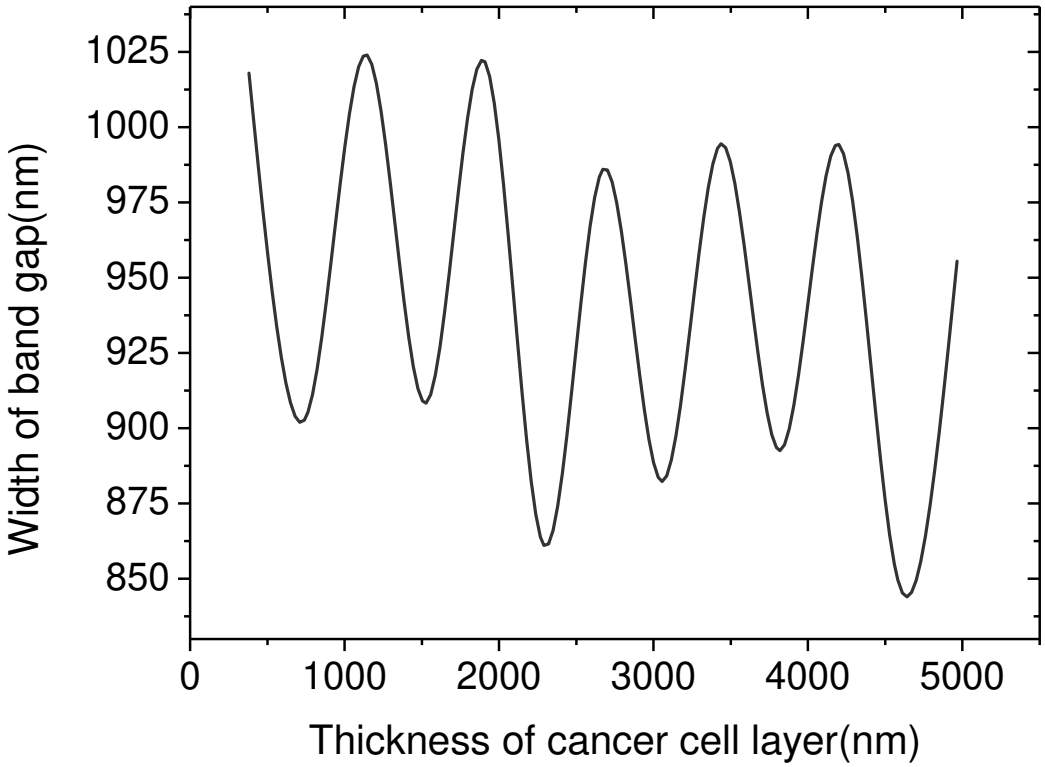

Fig. 10. Width of bandgap versus the cancer cell layer thickness of a binary photonic crystal for TE wave at d_1 = 117 nm, d_2 = 265 nm, n_1 = 3.3, n_2 = 1.46, $\theta_0 = 0°$ and N = 5.

3.5. Cancer cell sensor optimization

Figure 11 shows the defect modes corresponding to different cells at the sensitivity optimized conditions ($\theta_0 = 85°$, d_f = 13D and N = 3). When the normal cell is treated as a defect layer, the resonant peak position is at 1855.05 nm. It is found that resonant peak shifts to a higher wavelength region as cancerous cells are treated as defect layers. The new wavelength positions of the defect mode are cell-dependent. The new wavelength positions are at 1951.62, 1956.25, 1963.11, 1972.8 and 1976.68 nm for Jurkat, Hela, PC12, MDA-MB231 and MCF-7 cells, respectively. The sensitivity is found as 2414.25, 2409.52, 2401.4, 2390.4 and 2384.9 nm/RIU for the cells of Jurkat, Hela, PC12, MDA-MB231 and MCF-7, respectively. Table 14 presents the refractive indices of different cancerous cells, defect mode positions of each and the sensitivity of the proposed binary photonic crystal to each cell.

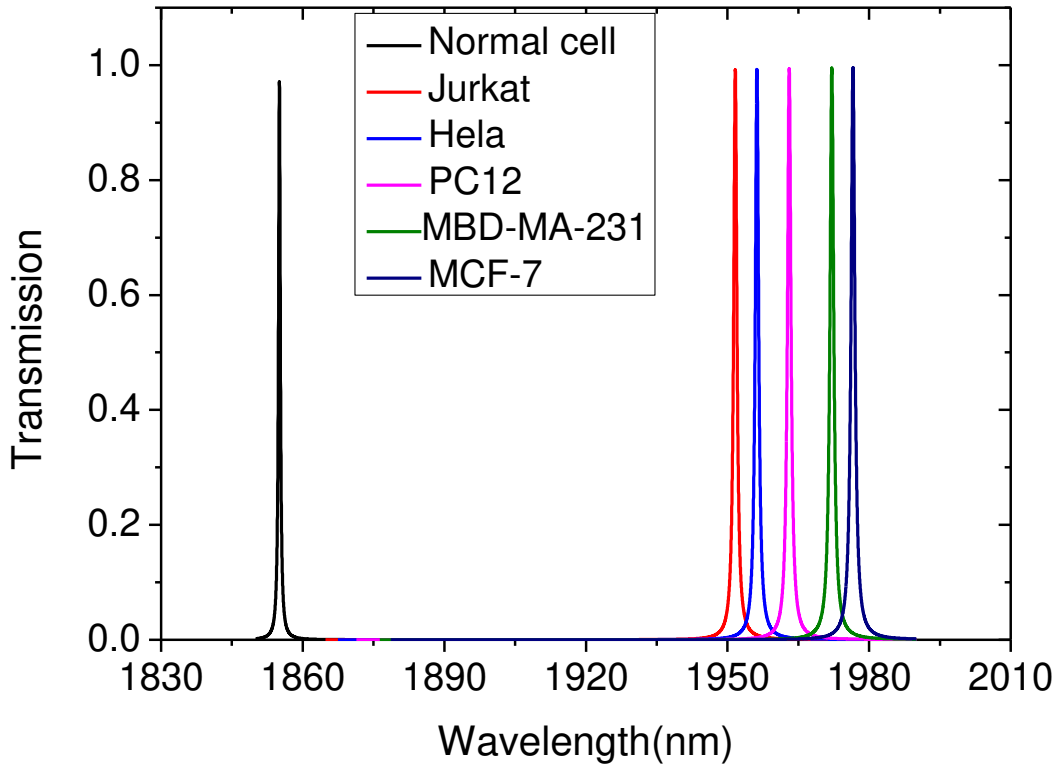

Fig. 11. Transmission spectra of a binary photonic crystal for TE wave at $\theta_0 = 85°$, $d_1 = 117$ nm, $d_2 = 265$ nm, $n_1 = 3.3$, $n_2 = 1.46$, d = 13D and N = 3.

Table 14. Defect mode position and sensitivity of the cancerous cells at $\theta_0 = 85°$, d = 13D and N = 3.

Cell	Refractive index	Wavelength (nm)	Wavelength shift (nm)	Sensitivity (nm/RIU)
Normal	1.350	1855.05	-	-
Jurkat	1.390	1951.62	96.57	2414.25

Hela	1.392	1956.25	101.2	2409.52
PC12	1.395	1963.11	108.06	2401.33
MDA-MB231	1.399	1972.18	117.13	2390.4
MCF-7	1.401	1976.68	121.63	2384.9
Average sensitivity = 2400.08 nm/RIU				

To show the efficiency of the proposed sensor, we calculated some performance parameters such as quality factor, figure of merit, detection limit, detection accuracy, signal-to-noise ratio, standard deviation, sensor resolution and dynamic range [15,16]. Table 15 shows the calculated values of the sensor performance parameters.

$$QF = \frac{\lambda_{peak}}{FWHM} \tag{14}$$

$$FOM = \frac{S}{FWHM} = \frac{\Delta\lambda}{\Delta n * FWHM} \tag{15}$$

$$DL = \left(\frac{FWHM}{\Delta\lambda}\right)^{\frac{5}{4}} \left(\frac{2\,\Delta n}{3}\right) \tag{16}$$

$$DA = \frac{1}{FWHM} \tag{17}$$

$$SNR = \frac{\Delta\lambda}{FWHM} \tag{18}$$

$$\sigma = \left(\frac{2}{9}\right)\left(\frac{FWHM}{SNR^{1/4}}\right) \tag{19}$$

$$\mathrm{SR} = \mathrm{S}\,(DL) = \frac{\Delta\lambda}{\Delta \mathrm{n}}\,(DL) \tag{20}$$

$$DR = \frac{\lambda_{peak}}{\sqrt{FWHM}} \tag{21}$$

Table 15. Performance parameters of the cancer cell sensor at optimized conditions ($\theta_0 = 85°$, d = 12D and N = 3).

	Normal	Jurkat	Hela	PC12	MDA-MB231	MCF-7
QF	4122.33	2439.52	2356.92	2256.44	2143.67	2059.04
DL	-	6.66×10^{-5}	6.91×10^{-5}	7.23×10^{-5}	7.63×10^{-5}	7.99×10^{-5}
SR	-	0.160	0.166	0.173	0.182	0.190
SNR	-	120.71	121.92	124.20	127.31	126.69

DR	2.76×10^3	2.18×10^3	2.14×10^3	2.1×10^3	2.05×10^3	2.01×10^3
DA	2.22	1.25	1.20	1.14	1.08	1.04
FOM	-	3017.81	2903.04	2760.15	2598.26	2484.27
σ_{peak}	-	6.47	6.76	7.19	7.74	8.05

Table 16 presents a comparison of the current work sensitivity with that of the most recent published biosensors. It shows the technique used and the sensitivity obtained. As can be seen, the current sensor achieves the highest sensitivity.

Table 16. Comparing the sensitivity of the current work with that of the most recent published biosensors.

Techniques/Structures	**Year**	**Sensitivity** (nm/RIU)	**References**
Gold coated circular PCF sensor	2017	2200	[17]
Square lattice of rods in SiO_2	2018	720	[18]
1D nano composite material coated photonic crystal	2019	43	[19]
1D PC that contains a defect layer	2019	2200	[20]
Array of split ring resonators	2019	658	[21]
A graphene meta-surface based sensitive infrared biosensor	2020	431	[22]
Square lattice defect-based PC sensor	2020	2360.12	[23]
1D binary PC	2021	344	[24]
1D binary PC that contains a defect layer	2021	2400.08	Current work

Conclusion

We have assumed a nano-detector using 1D binary PC to detect cancerous cells. The effects of incident angle, number of periods and the defect layer thickness on the sensitivity and bandgap width of the proposed structure were investigated. By changing the blood sample from normal to cancer cells, the defect mode is shifted to a higher wavelength region. The sensitivity of the proposed design is considerably enhanced when the incidence angle and the defect layer thickness increase. The photonic bandgap width of the proposed binary photonic crystal increases when the incidence angle increases while it oscillates as the defect layer thickness increases. When the number of periods increases, both sensitivity as well as bandgap width decrease. The sensitivity reached 2400.08 nm/RIU at optimized conditions which is extremely high when compared to most recent papers published in the biosensing field. In addition, our sensor has a very simple structure, tunable design and low cost.

Declarations

Competing Interests: The authors declare that they have no known competing financial interests or personal relationships that could have appeared to influence the work reported in this paper.
Funding Info: Arab Fund for Economic and Social Development.

Author contribution: All authors contributed to the study conception and design. Mathematical derivation and part of the editing were performed by [Malek G. Daher]. The code and part of the editing were performed by [Sofyan A. Taya] and [Ilhami Colak]. The first draft of the manuscript was written by [Shobhit K. Patel] and [Omar M. Ramahi]. Discussion of the results was performed by [Sofyan A Taya] and [Omar M. Ramahi]. All authors commented on previous versions of the manuscript. All authors read and approved the final manuscript.
Consent to Participate (Ethics): No consent to participate is required for this study.
Consent for Publish (Ethics): No consent for publication is required for this study.
Acknowledgement: The authors deeply acknowledge the financial support of the Arab Fund for Economic and Social Development.

References
[1] Rebecca Katz, Mat Edelson, The Cancer-Fighting Kitchen: Nourishing, Big-Flavor Recipes for Cancer, Ten Speed Press; Crown Publishing Group, New York, 2009
[2] S. Suresh, Biomechanics and biophysics of cancer cells, Acta Biomater 3 (4) (2007) 413–438.
[3] V. Backman, M.B. Wallace, L.T. Perelman, J.T. Arendt, R. Gurjar, M.G. Müller, Q. Zhang, G. Zonios, E. Kline, J.A. McGilligan, S. Shapshay, T. Valdez, K. Badizadegan, J.M. Crawford, M. Fitzmaurice, S. Kabani, H.S. Levin, M. Seiler, R.R. Dasari, I. Itzkan, J. Van Dam, M.S. Feld, T. McGillican, Detection of preinvasive cancer cells, Nature 406 (6791) (2000) 35–36.
[4] M. Danaie, B. Kiani, Design of a label-free photonic crystal refractive index sensor for biomedical applications, Photonics Nanostruct.-Fundam. Appl. 31 (2018) 89–98.
[5] Abinash Panda, Pukhrambam Puspa Devi, Photonic crystal biosensor for refractive index based cancerous cell detection, Optical Fiber Technology, Volume 54, 2020, 102123. https://doi.org/10.1016/j.yofte.2019.102123.
[6] Derbali, J., AbdelMalek, F., Obayya, S.S.A. *et al.* Design of a compact photonic crystal sensor. *Opt Quant Electron* **42,** 463–472 (2011). https://doi.org/10.1007/s11082-010-9429-4
[7] Vijayalakshmi, D., Manimegalai, C.T., Ayyanar, N. *et al.* Highly sensitive tri-path photonic crystal fiber plasmonic sensor based on hybrid layer of gold/platinum diselenide. *Opt Quant Electron* **53,** 454 (2021). https://doi.org/10.1007/s11082-021-03092-7
[8] Islam, M.R., Iftekher, A.N.M., Hasan, K.R. *et al.* Design and numerical analysis of a gold-coated photonic crystal fiber based refractive index sensor. *Opt Quant Electron* **53,** 112 (2021). https://doi.org/10.1007/s11082-021-02748-8
[9] A.N. Bashkatov, E.A. Genina, V.V. Tuchin, Optical properties of skin, subcutaneous, and muscle tissues: a review, J. Innovative Opt. Health Sci. 4 (2011) 9–38.
[10] A. Kim, B.C. Wilson, Measurement of Ex Vivo and In Vivo Tissue Optical Properties: Methods and Theories Optical-Thermal Response of Laser-Irradiated Tissue, chapter 8, second ed., Springer, Berlin, 2011.
[11] R. Barer, Refractometry and interferometry of living cells, J. Opt. Soc. Am. 47 (6) (1957) 545–556.
[12] N. Lue, G. Popescu, T. Ikeda, R.R. Dasari, K. Badizadegan, M.S. Feld, Live cell refractometry using microfluidic devices, Opt. Lett. 31 (18) (2006) 2759–2761.
[13] Woo June Choi, Do In Jeon, Sang-Gun Ahn, Jung-Hoon Yoon, Sungho Kim, Byeong Ha Lee, Full-field optical coherence microscopy for identifying live cancer cells by

quantitative measurement of refractive index distribution, Opt. Express 18 (22) (2010) 23285–23295.
[14] R. Dalmisa, O. Y. Keskina, N. F. Ak Azem, and I. Birlik, "A new one dimensional photonic crystal combination of TiO2/CuO form structural color applications", *Ceramics International*, Vol. 45, No. 17, pp. 21333-21340 (2019).

[15] A. M. Ahmed and M. Shaban, "Highly sensitive Au–Fe2O3–Au and Fe2O3–Au–Fe2O3 biosensors utilizing strong surface plasmon resonance", *Applied Physics B Lasers Optics*, Vol. 126, No. 4, pp. 1–10 (2020).

[16] A. M. Ahmed, H. A. Elsayed and A. Mehaney, "High-Performance Temperature Sensor Based on One-dimensional Pyroelectric Photonic Crystals Comprising Tamm /Fano Resonances", Plasmonics, Vol. 16, No. 2, pp. 547-557 (2021).

[17] M. Hasan, S. Akter, A. A. Rifat., S. Rana and S. Ali "A highly sensitive gold-coated photonic crystal fiber biosensor based on surface plasmon resonance", *Photonics*, Vol. 4, No. 1, pp. 18-28 (2017).
[18] M. Danaie, and B. Kiani, "Design of a label-free photonic crystal refractive index sensor for biomedical applications", *Photonics and Nanostructures – Fundamentals and Applications*, Vol. 31, No. 13, pp. 89-98 (2018).
[19] N. R. Ramanujam, I. Amiri, S. A. Taya, S. Olyaee, R. Udaiyakumar, A. P. Pandian, K. S. J. Wilson, P. Mahalakshmi and P. P. Yupapin, "Enhanced sensitivity of cancer cell using one dimensional nano composite material coated photonic crystal", *Microsystem Technologies,* Vol. 25, No. 1, pp.189-196 (2019).

[20] A. H. Arafa, and Z. A. Zaky, "Ultra-sensitive photonic crystal cancer cells sensor with a high-quality factor"*, Journal Pre-proofs,* Vol. 104, No. 4, p. 102991 (2019).

[21] H. E. Nejad, A. Mir and A. Farmani, "Supersensitive and Tunable Nano-Biosensor for Cancer Detection", *IEEE Sensors Journal,* Vol. 19, No. 13, pp. 4874-4881 (2019).
[22] S. Patel, J. Parmar, Y. Kosta, M. Ladumor, R. Zakaria, T. Nguyen, et al. "Design of graphene metasurface based sensitive infrared biosensor, Sens Actuators A Phys., Vol. 301, p. 111767 (2020).
[23] A. Panda and P. Devi, "Photonic crystal biosensor for refractive index based cancerous cell detection", *Optical Fiber Technology*, Vol. 54, No. 40, p.102123 (2020).
[24] K. M. Abohassan, H. S. Ashour and M. M. Abadla, "A 1D photonic crystal- based sensor for detection of cancerouse blood cells", Optical and Quantum Electronics, Vol. 53, No. 356, pp. (2021)